Journal of Alloys and Compounds 479 (2009) 82–86

Contents lists available at ScienceDirect

Journal of Alloys and Compounds

journal homepage: www.elsevier.com/locate/jallcom

The influence of *HS*-AlF_3 on the decomposition reaction of MgH_2

Johannes Noack, Gudrun Scholz, Stephan Rüdiger, Michael Feist, Erhard Kemnitz *

Institute of Chemistry, Humboldt University Berlin, Brook-Taylor-Street 2, 12489, Berlin, Germany

ARTICLE INFO

Article history:
Received 13 October 2008
Accepted 23 December 2008
Available online 7 February 2009

Keywords:
Hydrogen absorbing materials
Metal hydrides
Sol–gel processes
Gas–solid reactions
MAS NMR

ABSTRACT

The influence of nanoscopic aluminium fluoride prepared via a sol–gel-synthesis route developed by our group on the thermal decomposition of MgH_2 used as hydrogen storage material has been comprehensively investigated. Combined XRD and MAS NMR experiments have been performed to follow structural changes in ball milled MgH_2/*HS*-AlF_3 mixtures at thermal decomposition. Although the behaviour of Lewis acidic metal fluorides is discussed being catalytic, our results with *HS*-AlF_3 clearly give a different picture. We found strong evidence for a decrease of the decomposition temperature in combination with a significant acceleration of the decomposition rate; however, the action of at least AlF_3 is not catalytic in nature. As shown, a fluoride against hydride exchange is taking place, thus transforming AlF_3 irreversibly into AlH_3, which is followed by decomposition into metallic Al (MgAl alloy).

1. Introduction

Magnesium hydride is considered to be one of the most promising hydrides studied as hydrogen storage materials, due to its high gravimetric hydrogen capacity (7.6 wt.%), easy availability and low cost. However, a commercial use is limited so far, because the high thermodynamic stability (formation enthalpy $\Delta H_f = -75.3$ kJ/mol) requires decomposition temperatures above 300 °C. In addition the decomposition is hampered by its slow hydrogen evolution kinetics. To overcome these limitations a lot of work has focused on developing catalytic additives to improve the kinetic characteristics of the involved processes.

The introduction of structural defects and reduction of particle sizes to nanoscopic range, as obtained upon ball milling of magnesium hydride, results in enhanced reaction rates of the dehydrogenation [1,2]. In recent years, a lot of work has been focused on the addition of numerous transition metals [3], metal oxides [4] such as Nb_2O_5, V_2O_5, Ta_2O_5, and metal fluorides such as NbF_5, FeF_3, TiF_3 and NiF_2 [5–9] into the MgH_2 matrix to shift the hydrogenation/dehydrogenation reaction to lower temperatures and increase the rate of the reaction. Until now, the mechanism of this reaction and the exact influence of the catalytic additive is still under discussion. Unfortunately, Mg^0 and MgH_2 show high reactivity towards oxygen and water, so MgH_2 particles are usually covered by a MgO-surface layer. This has a negative influence on the reaction kinetics by limitation of hydrogen diffusion. Liu et al. [6] demonstrated that a fluorination of metal surfaces, accessible by reaction with fluoride containing aqueous solutions, might act as a protective coating for the particles. Fluorinated particle surfaces can act as a barrier to O_2, H_2O, CO, or N_2 while, on the other side, they may be permeable to H_2 through microcracks of the MgF_2 surface [10]. Since ball milling of magnesium hydride with metal oxides can lead to the formation of MgO and partial reduction of the oxide, a fluorination of the particle surfaces should be achieved by milling with metal fluorides instead. From this point of view, the use of metal fluorides should have definite advantages.

The use of Lewis acids for the activation of the H–H bond could result in higher reaction rates for hydrogen evolution at even lower temperatures. Computational studies have shown that the donation of H_2 σ-electron density into the low lying vacant valence orbitals of Mg^{2+} and Al^{3+} as bare ions can result in significant interaction energies [11]. Unfortunately, it is impossible to establish such bare ions in real solids. Energies for the interaction of hydrogen molecules with AlF_3 and MgF_2 in the gas phase have been calculated to be 11.3 and 11.8 kJ/mol, respectively [12]. High surface (*HS*) metal fluorides, e.g. *HS*-MgF_2 and *HS*-AlF_3, should be excellent catalysts to overcome the aforementioned problems. We have developed a sol–gel synthesis route to highly disordered, X-ray amorphous and high surface metal fluorides [13].

In this work, *HS*-AlF_3 prepared this way and exhibiting strong Lewis acidity, has been investigated regarding its impact on the decomposition of MgH_2. In contrast to metal fluorides investigated so far in this respect, local structures of AlF_3 are easily accessible by ^{19}F and ^{27}Al MAS NMR. This gives the opportunity to follow changes and to identify intermediates that occur from high-energy ball milling and during the thermally induced decomposition reaction. Finally, an approach to the role of *HS*-AlF_3 in these processes should be possible.

* Corresponding author. Tel.: +49 30 2093 7555; fax: +49 30 2093 7277.
E-mail address: erhard.kemnitz@chemie.hu.berlin.de (E. Kemnitz).

0925-8388/$ – see front matter © 2009 Published by Elsevier B.V.
doi:10.1016/j.jallcom.2008.12.154

2. Experimental

All operations in synthesis and milling were performed under argon as inert atmosphere using Schlenk techniques or a glove box. *HS*-AlF_3 was obtained by fluorination of Al(O*i*Pr)$_3$ dissolved in *i*-PrOH with HF/*i*PrOH in a sol–gel synthesis described elsewhere [14,15]. Samples were prepared by mechanical milling of MgH_2 (Alfa Aesar; 98%) with different ratios of *HS*-AlF_3 (0.5, 3, 17 mol%) using a planetary mill (Fritsch Pulverisette P7). Each 45 ml syalon vial was filled with 1 g solid. Milling was performed for 4 h with five syalon balls of 2.9 g each (mass ratio of balls/sample = 14.5:1) at 600 rpm under inert gas atmosphere.

XRD measurements were carried out on a Seiffert XRD 3003 TT diffractometer (Freiberg, Germany) with CuK_α radiation. The samples were prepared in a glove box and were covered with a special X-ray amorphous polystyrene foil to avoid the reaction with air. Phases were identified by comparison with the ICSD powder diffraction file [16]. ^{19}F and ^{27}Al MAS NMR spectra have been recorded on a Bruker AVANCE 400 spectrometer at a rotation frequency of 25 kHz using a 2.5 mm MAS probe. The resonance frequencies have been 376.4 MHz for ^{19}F and 104.6 MHz for ^{27}Al; chemical shifts are given relative to $CFCl_3$ for ^{19}F and $AlCl_3$ (1 M in water) for ^{27}Al. ^{27}Al and ^{19}F spectra were simulated using dmfit2007 [17]. The thermal dehydrogenation behaviour was studied by using a NETZSCH thermoanalyzer STA 409 C [DTA-TG sample carrier system; corundum crucibles (baker 0.8 ml); Pt/PtRh10 thermocouples; sample mass 15–30 mg; empty reference crucible; constant purge gas flow of 70 ml/min hydrogen (MESSER-GRIESHEIM 4.8); heating rate 10 K/min for dynamic treatment, if necessary followed by various isothermal segments set at appropriate temperatures between 250 and 420 °C]. The temperature evaluation of the DTA curves regarding initial (T_i), extrapolated onset (T_{on}^{ex}), and peak (T_P) temperatures was performed following international recommendations [25].

3. Results

Structural analysis was performed before and after decomposition at 320 °C by means of X-ray diffractometry and MAS NMR spectroscopy. Fig. 1 shows the XRD patterns of MgH_2 with 17 mol% *HS*-AlF_3 of the as-milled sample prior (a) and after (b) decomposition at 320 °C. The Bragg-reflections in the X-ray diffractogram of the as-milled sample reveal the presence of tetragonal β-MgH_2 (PDF 12-0697) as the main component. The existence of the metastable orthorhombic γ-MgH_2-phase, which has been previously reported [1] to be formed on milling, could not be observed under these conditions. *HS*-AlF_3 is a highly disordered, nanoscopic solid and is therefore not detectable by X-ray diffraction. In addition, increasing amounts of metallic magnesium (PDF 35-0821) can be identified as a product of milling-induced decomposition of the hydride.

After thermal treatment of the sample (pattern b), magnesium hydride reflections disappear completely and metallic magnesium as a product of decomposition can be identified. A fluorinating action of AlF_3 during thermal treatment can be deduced from the reflections of MgF_2 in the diffractogram. The reflection at 36° points out the formation of MgAl alloys upon decomposition of the MgH_2/*HS*-AlF_3 sample.

The observation of chemical reactions by XRD measurements is limited by the crystallite size of the sample and is therefore not applicable for amorphous or nanocrystalline particles as obtained by ball milling. Solid state NMR is a powerful method which also gives insight into the local structure of X-ray amorphous samples. In

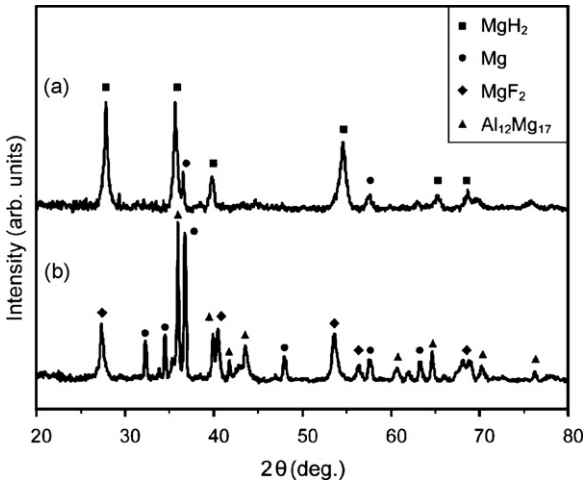

Fig. 1. XRD patterns of a ball milled mixture of MgH_2 with 17 mol% *HS*-AlF_3 (a), and after subsequent thermal decomposition at 320 °C (b).

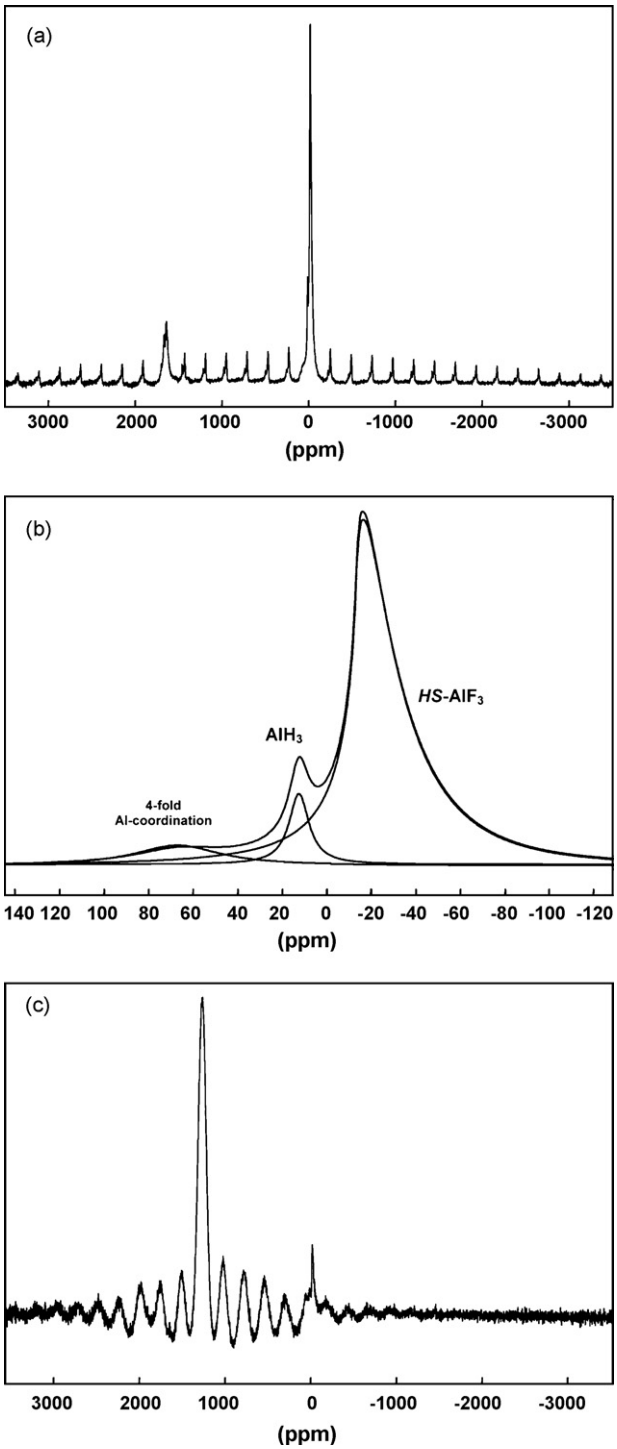

Fig. 2. ^{27}Al MAS NMR spectra of (a) a ball milled mixture of MgH_2 with 17 mol% *HS*-AlF_3, (number of accumulations (na): 66688); (b) enlargement of the central signals of (a) together with their deconvolution: $\delta_{27Al1} = -13.3$ ppm (78%), $\delta_{27Al2} = 12.5$ ppm (12%), $\delta_{27Al3} = 67.0$ ppm (10%); (c) the same sample thermally treated at 320 °C, (na: 72000).

the case of the ball milled samples of MgH_2 with different amounts of *HS*-AlF_3, ^{19}F and ^{27}Al MAS NMR measurements were applied for characterisation of the solids. For ^{1}H see supporting information.

The ^{27}Al MAS NMR spectrum (Fig. 2) of an MgH_2 sample which has been milled for 4 h with 17 mol% *HS*-AlF_3 allows the assignment of at least three different species. Spectrum (a) shows the region from −3500 to 3500 ppm. At 1638 ppm a signal is observed which can be assigned to metallic aluminium Al^0. The chemical shift values of Al(III) compounds are usually in the region around 0 ppm. This region is given as enlargement in Fig. 2b. The major signal is the typical ^{27}Al signal of *HS*-AlF_3 with δ_{27Al} at −18.9 ppm [15]. In agreement with Hwang et al. [18] the symmetrical line at 12.5 ppm can be attributed to AlH_3. At 67.0 ppm an additional broad signal can be interpolated which lies in the region of four-fold coordinated aluminium sites. The integral proportions of the different species are given in the caption to Fig. 2.

On decomposition of this sample at 320 °C, the *HS*-AlF_3 signal in the ^{27}Al MAS NMR spectrum (Fig. 2c) disappears almost completely. The signal belonging to Al^0 remains with decreased intensity after thermal treatment. A new line dominating the spectrum can be observed at 1265 ppm. Samples with lower *HS*-AlF_3 content show an emerging line at 1916 ppm after dehydrogenation, which is illustrated for the case of 3 mol% *HS*-AlF_3 in Fig. 3b.

Similarly, the ^{19}F MAS NMR spectrum (Fig. 4a) obtained after milling of MgH_2 with 17 mol% *HS*-AlF_3 for 4 h shows the ^{19}F signal of *HS*-AlF_3 as the main component at −168.3 ppm. On the right hand side of the signal, further species can be interpolated belonging to additional, so far unidentified species and MgF_2 (δ_{19F} = −198.0 ppm). The existence of hydride fluorides such as AlF_xH_{3-x} or MgF_xH_{2-x} cannot be ruled out.

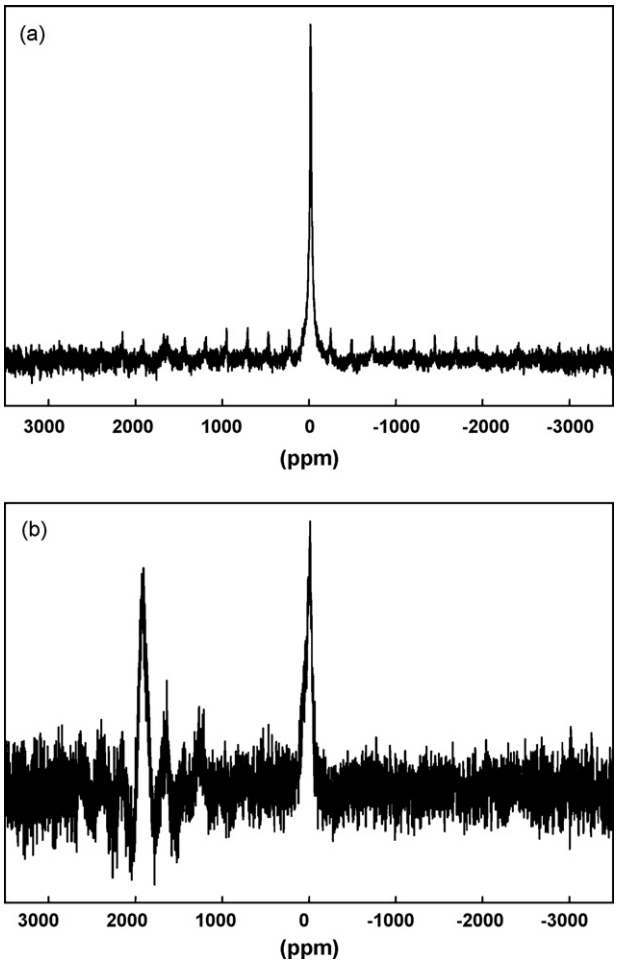

Fig. 3. ^{27}Al MAS NMR spectra of (a) a ball milled mixture of MgH_2 with 3 mol% *HS*-AlF_3 (na: 68277); (b) the same sample after thermal decomposition at 320 °C (na: 72000).

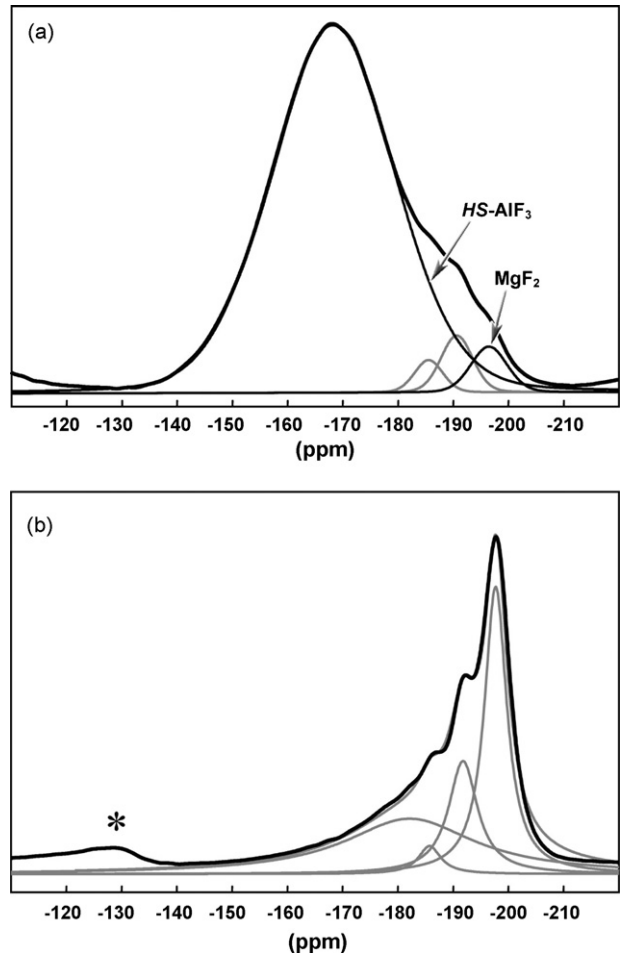

Fig. 4. ^{19}F MAS NMR spectra (central lines and their deconvolutions) of (a) a ball milled mixture of MgH_2 with 17 mol% *HS*-AlF_3: δ_{19F1} = −196.4 ppm (3%), δ_{19F2} = −191.1 ppm (4%), δ_{19F3} = −186.4 ppm (3%), δ_{19F4} = −168.1 ppm (90%); and (b) the same sample thermally treated at 320 °C: δ_{19F1} = −197.7 ppm (37%), δ_{19F2} = −191.8 ppm (18%), δ_{19F3} = −185.8 ppm (4%), δ_{19F4} = −182.2 ppm (41%); *: spinning side band.

After dehydrogenation of this sample at 320 °C (Fig. 4b), the ^{19}F signal belonging to *HS*-AlF_3 signal vanishes almost completely. The signals at −186, −192 and −198 ppm, respectively, remain under these conditions (cf. Fig. 4b).

The thermal decomposition of the as-milled MgH_2 can be followed via the DTA curves upon heating at 10 K/min in pure hydrogen atmosphere (Fig. 5). The untreated MgH_2 sample starts to decompose at about 420 °C which causes a sharp endothermal DTA signal with an extrapolated onset temperature (T_{on}^{ex}) of 436 °C and a peak temperature (T_P) of 480 °C under these experimental conditions. Ball milling of this MgH_2 sample results in particle size reduction as can be seen from the broadening of the X-ray reflections (not shown). As a consequence, T_{on}^{ex} for the decomposition reaction decreased to 350 °C (T_P 384 °C). A further shift to lower temperatures is observed for the dissociation of samples containing 3 and 17 mol% of *HS*-AlF_3. Addition of 0.3 mol% *HS*-AlF_3 has a very little effect on the decomposition reaction, but 3 mol% and more has a direct impact on the thermal behaviour of MgH_2. It is noteworthy mentioning that both samples (3 and 17 mol% *HS*-AlF_3) show almost the same DTA signal upon heating (T_{on}^{ex} 290, T_P 360 °C). This means that further increasing the amount of added *HS*-AlF_3 (more than

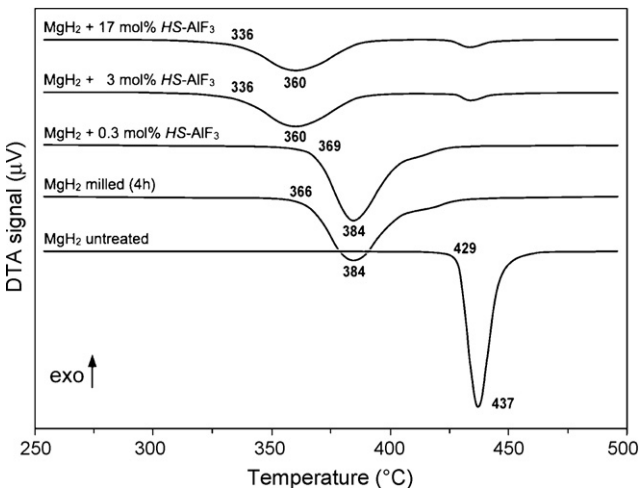

Fig. 5. DTA curves of MgH_2 samples milled with different amounts of *HS*-AlF_3 in pure hydrogen, normalised on hydrogen content.

3 mol%) does not lead to a stronger decrease of the decomposition temperature.

4. Discussion

Due to the small crystallite sizes, the identification of chemical reactions or phase transformations induced by high-energy ball milling only by XRD analysis of the as-milled samples is not possible. Together with ^{19}F and ^{27}Al MAS NMR experiments however, clear evidence can be given for the existence of Mg^0, MgH_2, AlF_3, Al^0, AlH_3, MgF_2 and further so far unidentified ^{19}F species already in the milled samples.

From the ^{19}F and ^{27}Al MAS NMR spectra it can be deduced, that a partial fluoride–hydride exchange reaction is already taking place during ball milling of MgH_2 with *HS*-AlF_3, clearly shown by the formation of MgF_2 and AlH_3 (Figs. 2b and 4a). Taking the enthalpies of formation (ΔH_f°) for MgH_2, MgF_2, AlF_3 and AlH_3 into account, which are −75.3, −1124.2, −1510.4 and −46.0 kJ/mol, respectively [19], a total reaction enthalpy, ΔH°, of −217.9 kJ/mol can be estimated for the reaction given in Eq. (1).

$$3MgH_2 + 2HS\text{-}AlF_3 \xrightarrow{\text{milling}} 3MgF_2 + 2AlH_3 \quad (1)$$

Bearing in mind that surface energies of nanoscopic solids might be significantly higher than those of crystalline compounds, this reaction should be possible from the thermodynamic point of view. Although this reaction is thermodynamically favoured it is far from being quantitative. Even after milling, *HS*-AlF_3 is the main fluoride component in the matrix (see Figs. 2a,b, 3a, 4a).

Apart from AlH_3, which is formed by milling of *HS*-AlF_3 with MgH_2, the broad signal at 67.0 ppm in the ^{27}Al MAS NMR spectrum (Fig. 2b) can be possibly assigned to $Mg(AlH_4)_2$. It could either be formed from the binary hydrides during the milling procedure (Eq. (2a)) or in a direct metathesis reaction (Eq. (2b)) which is known from milling of $AlCl_3$ with MgH_2 [20].

$$MgH_2 + 2AlH_3 \xrightarrow{\text{milling}} Mg(AlH_4)_2 \quad (2a)$$

$$4MgH_2 + 2HS\text{-}AlH_3 \xrightarrow{\text{milling}} Mg(AlH_4)_2 + 3MgF_2 \quad (2b)$$

As a consequence of the H/F substitution, the resulting alane or alanate can be easily decomposed to metallic aluminium and hydrogen by mechanical impact (Eq. (3a)) or by thermal treatment (Eq. (3b)). This reaction is indicated by the signal of metallic aluminium at 1638 ppm in the ^{27}Al MAS NMR experiment (Fig. 2a).

$$AlH_3 \xrightarrow{\text{milling}} Al^0 + 3/2H_2 \quad (3a)$$

$$Mg(AlH_4)_2 \xrightarrow{\text{milling}} MgH_2 + 2Al^0 + 3H_2 \quad (3b)$$

Both XRD and ^{27}Al MAS NMR prove that Mg and Al form an alloy upon thermal decomposition. Depending on the content of *HS*-AlF_3 in the sample, the stoichiometry of the Mg_xAl_y alloy varies. The alloy obtained after decomposition of MgH_2 with 17 mol% *HS*-AlF_3 as presented in Fig. 2c induces a ^{27}Al NMR chemical shift of 1265 ppm. According to Bastow and Smith [21] this NMR shift could be assigned to an Al-rich alloy with the stoichiometry $Mg_{17}Al_{12}$. With lower Al contents, the formation of an Mg-rich alloy with 6 wt.% Al is observed, which is illustrated in Fig. 3b for the case of 3 mol% *HS*-AlF_3 content in the MgH_2 sample.

Moreover, the fluoride transfer according to Eq. (1) is enhanced during the decomposition of the MgH_2/*HS*-AlF_3 sample and the content of *HS*-AlF_3 is dramatically reduced.

The DTA results shown in Fig. 5 give clear evidence for the effect of the addition of strongly Lewis acidic nanoscopic AlF_3 as the decomposition temperature is significantly decreased by about 25 K. Obviously amounts of 3 mol% AlF_3 are sufficient enough to induce this effect.

We have also performed kinetic measurements for the decomposition (see supporting information) of pure MgH_2 and MgH_2/*HS*-AlF_3 mixtures and have calculated the activation energies (E_a) from the rate constants at different temperatures applying a nucleation and growth model [22]. These values confirm the effect of milling and *HS*-AlF_3 addition, respectively, as already displayed above: the E_a values are 184 kJ/mol for pure MgH_2, 154 kJ/mol for milled MgH_2 and 124 kJ/mol for MgH_2/AlF_3. Data for the activation of the MgH_2 decomposition given in the literature deviate from 91 to 156 kJ/mol [1,23]. Hence, the obtained values clearly have a strong dependence on the detailed procedure and the kinetic model applied. However, since these kinetic investigations were performed under the same conditions, the data clearly give evidence that addition of strongly Lewis acidic AlF_3 reduces the activation energy and, consequently, significantly improves the decomposition rate. This effect might have two different origins. At first, due to extraordinary high Lewis acidity, hydrogen atoms might be transferred to *HS*-AlF_3 sites on the particle surfaces, which then combine to hydrogen gas. Second, metallic magnesium, that is formed on dissociation of the hydride, is thermodynamically stabilised by alloying. As a consequence of this, the corresponding MgH_2 is destabilised and the decomposition occurs at a lower temperature [24].

5. Conclusion

Combined XRD and MAS NMR experiments allowed to follow structural changes in ball milled MgH_2/*HS*-AlF_3 mixtures at thermal decomposition.

Although the addition of Lewis acidic metal fluorides in literature is discussed as being catalytic, our results with *HS*-AlF_3 clearly give a different picture. We found strong evidence for a decrease of the decomposition temperature in combination with a significant acceleration of the decomposition rate; however, the action of – at least AlF_3 – is not catalytic in nature. As shown, a fluoride against hydride exchange is taking place, thus transforming AlF_3 irreversibly into AlH_3, which is followed by decomposition into metallic Al (MgAl alloy). Fortunately this reaction is far from being stoichiometric, therefore several cycles might be performed for hydrogen storage but it is running into a “dead end”. We suspect that other metal fluorides will show very similar behaviour and so their action should be investigated in more detail too in order to

gain a better understanding of the rule of Lewis acid addition in general but especially in case of metal fluorides.

Acknowledgements

The authors would like to thank Mrs. S. Bäßler for performing the thermoanalytical measurements.

Appendix A. Supplementary data

Supplementary data associated with this article can be found, in the online version, at doi:10.1016/j.jallcom.2008.12.154.

References

[1] J. Huot, G. Liang, S. Boily, A. Van Neste, R. Schulz, J. Alloys Compd. 293 (1999) 495–500.
[2] A. Zaluska, L. Zaluski, J.O. Ström-Olsen, J. Alloys Compd. 288 (1999) 217–225.
[3] G. Liang, J. Huot, S. Boily, A. Van Neste, R. Schulz, J. Alloys Compd. 292 (1999) 247–252.
[4] G. Barkhordarian, T. Klassen, R. Bormann, J. Phys. Chem. B 110 (2006) 11020–11024.
[5] S.-A. Jin, J.-H. Shima, Y.W. Choa, K.-W. Yi, J. Power Sources 172 (2007) 859–862.
[6] F.-J. Liu, S. Suda, J. Alloys Compd. 231 (1995) 742–750.
[7] J.F.R. de Castro, A.R. Yavari, A. LeMoulec, T.T. Ishikawa, W.J. Botta, J. Alloys Compd. 389 (2005) 270–274.
[8] S. Deledda, A. Borissova, C. Poinsignon, W.J. Botta, M. Dornheim, T. Klassen, J. Alloys Compd. 404–406 (2005) 409–412.
[9] N. Recham, V.V. Bhat, M. Kandavel, L. Aymard, J.-M. Tarascon, A. Rougier, J. Alloys Compd. 464 (2008) 377–382.
[10] F.-J. Liu, S. Suda, J. Alloys Compd. 231 (1995) 742–750.
[11] R.C. Lochan, M. Head-Gordon, Phys. Chem. Chem. Phys. 8 (2006) 1357–1370.
[12] C.A. Nicolaides, E.D. Simandiras, Chem. Phys. Lett. 196 (1992) 213–219.
[13] St. Rüdiger, E. Kemnitz, Dalton Trans. 9 (2008) 1117–1127.
[14] E. Kemnitz, U. Groß, St. Rüdiger, S. Chandra Shekar, Angew. Chem. 115 (2003) 4383–4386;
E. Kemnitz, U. Groß, St. Rüdiger, S. Chandra Shekar, Angew. Chem. Int. Ed. 42 (2003) 4251–4254.
[15] St. Rüdiger, G. Eltanany, U. Groß, E. Kemnitz, J. Sol–Gel. Sci. Technol. 41 (2007) 299–311.
[16] JCPDS-ICDD – International Centre for Diffraction Data: PDF-2 Database (Sets 1-51 plus 70-89), PA 19073-3273 U.S.A., Release 2001, – PCPDFWIN Version 2.2.
[17] D. Massiot, F. Fayon, M. Capron, I. King, S. Le Calve, B. Alonso, J.O. Durand, B. Bujoli, Z.H. Gan, G. Hoatson, Magn. Reson. Chem. 40 (2002) 70–76.
[18] S.-J. Hwang, R.C. Bowman, J. Graetz, J.J. Reilly, W. Langley, C.M. Jensen, J. Alloys Compd. 446–447 (2007) 290–295;
S.-J. Hwang, R.C. Bowman, J. Graetz, J.J. Reilly, in: J.C.F. Wang, W. Tumas, A. Rougier, M. J. Heben, E. Akiba, (Eds.), Hydrogen Storage Materials, Mater. Res. Soc. Symp. Proc. Warrendale, PA, 2006, vol. 927E, 0927.
[19] D.R. Lide (Ed.), Handbook of Chemistry and Physics, 76th ed., CRC Press, Boca Raton, FL, USA, 1995.
[20] T.N. Dymova, N.N. Mal'tseva, V.N. Konoplev, A.I. Golovanova, D.P. Aleksandrov, A.S. Sizareva, Russ. J. Coord. Chem. 29 (2003) 385–389.
[21] T.J. Bastow, M.E. Smith, J. Phys. Condens. Matter. 7 (1995) 4929–4937.
[22] J.F. Fernández, C.R. Sánchez, J. Alloys Compd. 340 (2002) 189–198.
[23] H. Kawano, Y. Zhu, A. Tanaka, S. Sugimoto, Thermochim. Acta 371 (2001) 155–161.
[24] J.J. Vajo, T.T. Salguero, A.F. Gross, S.L. Skeith, G.L. Olson, J. Alloys Compd. 446–447 (2007) 409–414.
[25] J. O. Hill (Ed.), For Better Thermal Analysis III, Special edition of the International Confederation for Thermal Analysis (ICTA), 1991.